Curcumin induces and enhances the PARP1-mediated parthanatos in diffuse large B cell lymphoma

YAYUN WANG[1-3*], RUILI QI[1-3*], XUANZHU ZHAO[1-3], HANWEI MEI[1-4], MINGHAN QIU[2,3,5], FENGTING LIU[3] and HUAQING WANG[1-3]

[1]School of Integrative Medicine, Tianjin University of Traditional Chinese Medicine, Tianjin 301617, P.R. China; [2]Department of Oncology, Tianjin Union Medical Center, The First Affiliated Hospital of Nankai University, Tianjin 300121, P.R. China; [3]Tianjin Cancer Institute of Integrative Traditional Chinese and Western Medicine, Tianjin Union Medical Center of Nankai University, Tianjin 300121, P.R. China; [4]Department of Gastrointestinal Surgery 3, Tianjin Nankai Hospital, Tianjin Medical University, Tianjin 301617, P.R. China; [5]School of Medicine, Nankai University, Tianjin 300071, P.R. China

Received October 24, 2025; Accepted February 9, 2026

DOI: 10.3892/ol.2026.15554

Abstract. Diffuse large B-cell lymphoma (DLBCL) is the most common subtype of non-Hodgkin lymphoma in adults. Although the development and application of novel therapeutic agents have improved patient survival, primary drug resistance and the management of relapsed/refractory disease remain major challenges. Curcumin, a natural polyphenol, exhibits broad-spectrum antitumor activity. However, its anti-DLBCL efficacy and underlying mechanisms have not been well characterized. The present study investigated whether curcumin inhibited DLBCL by inducing parthanatos, a form of programmed cell death. Results showed that curcumin exerted a concentration-dependent, caspase-independent cytotoxic effect on DLBCL cells, accompanied by an increase in DAPI-positive/propidium iodide-positive cells. Western blotting analysis revealed that curcumin upregulated poly(ADP-ribose) and poly(ADP-ribose) polymerase 1 (PARP-1) expression in whole-cell lysates. Moreover, nuclear expression levels of apoptosis-inducing factor (AIF) and macrophage migration inhibitory factor were significantly elevated compared with their cytoplasmic levels. Immunofluorescence staining further confirmed the increased nuclear localization of PARP-1 and AIF. Furthermore, low-dose curcumin combined with ultraviolet B (UVB) irradiation synergistically induced parthanatos in DLBCL cells. Notably, olaparib, a specific PARP-1 inhibitor, attenuated activation of parthanatos induced by curcumin alone or in combination with UVB. In summary, the present findings suggest that curcumin inhibits DLBCL cell proliferation through PARP1-mediated parthanatos and exhibits synergistic effects with UVB irradiation.

Correspondence to: Professor Huaqing Wang or Professor Fengting Liu, Tianjin Cancer Institute of Integrative Traditional Chinese and Western Medicine, Tianjin Union Medical Center of Nankai University, 190 Jieyuan Avenue, Tianjin 300121, P.R. China
E-mail: huaqingw@163.com
E-mail: liufengting@tjmuch.com

*Contributed equally

Key words: curcumin, parthanatos, diffuse large B-cell lymphoma, poly (ADP-ribose) polymerase 1, DNA damage repair, radiosensitization

Introduction

Diffuse large B-cell lymphoma (DLBCL), the most common aggressive subtype of non-Hodgkin lymphoma (NHL), accounts for 30-40% of newly diagnosed cases globally. The 5-year overall survival rates range from 20 to 30% (1). R-CHOP chemotherapy, the standard first-line immunochemotherapy regimen for diffuse large B-cell lymphoma (DLBCL) comprising rituximab (R), cyclophosphamide (C), doxorubicin (H), vincristine (O) and prednisone (P), achieves durable remission in ~60% of patients. However, 30-40% of patients develop relapsed or refractory (R/R) disease, with a subsequent median overall survival of only 6-12 months (2). Conventional chemotherapy is often associated with poor patient tolerance, prolonged treatment duration and notable toxicity (2,3). Research efforts have increasingly focused on addressing these clinical challenges and improving patient outcomes in DLBCL (3). Resistance mechanisms to R-CHOP are multifaceted, including CD20 downregulation, MYC and BCL-2 co-expression, upregulation of anti-apoptotic proteins, constitutive activation of NF-κB and ERK pathways and TP53 mutations (4,5). Overcoming this resistance requires exploring alternative cell death pathways and combining novel agents, such as natural compounds from traditional medicine, with conventional therapies such as radiotherapy.

In the era of gene editing and artificial intelligence, traditional Chinese medicine (TCM) has gained renewed attention because of its holistic approach and unique therapeutic wisdom. Previous studies on TCM-derived compounds have revealed novel avenues of modern medicine. For instance, tanshinone inhibits vascular endothelial growth factor and

angiogenesis (6), safranin modulates gut microbiota and ameliorates metabolic syndrome (7) and curcumin has demonstrated anticancer potential via epigenetic modulation (8,9). Curcumin, a natural polyphenol derived from the rhizome of *Curcuma longa* (Zingiberaceae), is the primary active component of turmeric, which is a TCM (10). Turmeric was first documented in the 'Xinxiu Ben Cao' (Newly Revised Materia Medica) during the Tang Dynasty (11). Curcumin, a natural polyphenol, curcumin has garnered considerable interest because of its broad-spectrum antitumor activity (12). It modulates multiple signaling pathways by inhibiting NF-κB and STAT3, downregulating BCL-2 and activating caspase-dependent apoptosis (13,14). Curcumin exhibits a wide range of pharmacological activities, including anti-inflammatory (15), antibacterial (16), antioxidant (17), antitumor (inhibiting proliferation and metastasis) (8), radiosensitizing and chemosensitizing (18) and photobiological effects (19). It can also induce multiple modes of cell death, including apoptosis (20), autophagy (21), necrosis (22), necroptosis (23) and ferroptosis (24). Its anticancer efficacy has been demonstrated in both solid tumors (such as lung, colorectal and liver cancers) and hematological malignancies (such as leukemia and lymphoma) (25,26). Epigenetically, curcumin influences tumor progression by inhibiting histone acetyltransferases and modulating microRNA expression (27). Advanced delivery systems (such as liposomes and nanoparticles) improve its tumor-targeting efficiency and therapeutic efficacy (28). In lymphoma, curcumin has been shown to overcome bortezomib resistance (29) and enhance radiosensitivity (30), indicating its potential as a treatment for DLBCL treatment. However, the mechanism by which curcumin induces non-apoptotic cell death, in particularly parthanatos, remains poorly understood, and research in this area is limited. Thus, critical knowledge gaps regarding its application in DLBCL therapy remain to be addressed.

According to the Cell Death Nomenclature Committee, cell death can be classified based on morphological, biochemical and functional criteria (31). Physiologically regulated programmed cell death includes apoptosis, necroptosis, parthanatos, autophagy, ferroptosis and cyclophilin D-dependent necrosis (31). Parthanatos was first described by Wang *et al* (32) in 2009. Initially characterized in the context of neurodegenerative diseases (32-35), its relevance has been increasingly recognized in oncology, with roles identified in neuroblastoma (35), lung cancer (36), breast cancer (37), hepatocellular carcinoma (38), colon cancer (5), prostate cancer (39), leukemia (40) and myeloma (41). It is characterized by rapid poly(ADP-ribose) (PAR) polymerase 1 (PARP-1) activation, PAR polymer accumulation, apoptosis-inducing factor (AIF)/macrophage migration inhibitory factor (MIF) nuclear translocation and extensive DNA fragmentation (42). Parthanatos is a distinct form of programmed cell death that depends on PARP-1 and has been previously characterized (31). Unlike apoptosis and necrosis, parthanatos does not involve cellular swelling, apoptotic body formation or autophagosome accumulation. It is characterized by excessive cytoplasmic accumulation of PAR polymers. This accumulation leads to loss of mitochondrial membrane potential, translocation of AIF to the nucleus and extensive DNA fragmentation, resulting in cell death (38). This pathway has been extensively studied in neurodegenerative diseases (43). In oncology, parthanatos can be triggered by DNA-damaging agents (such as temozolomide) or PARP inhibitors, offering a therapeutic advantage in p53-deficient tumors (5,42). Recent studies have indicated that natural compounds (such as tanshinone) can induce parthanatos in leukemia cells (4,6). However, systematic studies of parthanatos in DLBCL are lacking.

Materials and methods

Cells and reagents. The human DLBCL cell lines SU-DHL-4, SU-DHL-6, SU-DHL-8, SU-DHL-10 and DoHH2 were provided by Professor Fengting Liu. Curcumin and Q-VD-OPh were obtained from MedChemExpress and olaparib was acquired from Selleck Chemicals.

Preparation and storage of experimental drugs. To ensure consistent drug concentrations and maintained bioactivity under experimental conditions, the storage and preparation protocols for all drugs used in the present study were standardized. Curcumin, Q-VD-OPh and olaparib were dissolved in dimethyl sulfoxide (DMSO) to prepare stock solutions of 50, 1 and 50 mM, respectively. Aliquots were stored at -80˚C in a cryogenic freezer. Working concentrations were prepared by diluting in complete RPMI-1640 medium (Gibco; Thermo Fisher Scientific, Inc.) immediately before use.

Cell thawing and recovery. To ensure that post-thaw cells retained their original biological functions, morphology and capacity for normal proliferation and metabolism-thereby providing a stable and healthy cellular source for subsequent culture and pharmacological assays-the cryopreservation and thawing procedures were carefully optimized. The cells were recovered using standard cryopreservation reversal procedures. Briefly, the water bath was pre-warmed to 37˚C. Cryovials containing frozen cells were promptly removed from the liquid nitrogen and immersed in a water bath with gentle agitation to accelerate thawing. After thawing, the external surfaces of the cryovials were wiped with 75% ethanol and transferred to a biological safety cabinet. The cell suspension was transferred into a centrifuge tube containing 5 ml pre-warmed complete medium [RPMI-1640 basal medium + 10% fetal bovine serum (FBS; ZETA Life) + 1% penicillin-streptomycin (dual antibiotics); pre-warmed to 37˚C), followed by centrifugation at 200 x g for 5 min at room temperature. The supernatant was carefully aspirated and the cell pellet was gently resuspended in fresh complete medium (RPMI-1640 basal medium + 10% FBS + 1% penicillin-streptomycin). The resuspended cells were then transferred into a labeled culture flask and incubated in an upright position in a humidified incubator maintained at 37˚C with 5% CO_2.

Cell culture and passaging. To maintain cells in the logarithmic growth phase and ensure consistent cell state and absence of contamination during experiments, cell culture and subculturing were performed according to the following standard procedures.

Cell lines (SU-DHL-8, SU-DHL-10 and DoHH2) were maintained in RPMI-1640 (Gibco; Thermo Fisher Scientific, Inc.) medium containing 10% FBS (ZETA Life) and 1%

penicillin-streptomycin at 37˚C in a humidified 5% CO_2 incubator. The cells were routinely monitored for growth, medium clarity and signs of contamination. Depending on the cell condition, the culture medium was replaced every 2-3 days to prevent bacterial contamination. All cell lines used in the present study were suspension cultures. At a high density, the cells formed aggregates and the medium became turbid upon gentle agitation. The cells were subcultured or diluted when reaching to appropriate densities to maintain exponential growth.

Cell proliferation activity assay: Cell Counting Kit-8 (CCK-8) method. To evaluate the inhibitory effect of curcumin on DLBCL cell proliferation and calculate its IC_{50} values, the following procedures were performed: SU-DHL-8 and SU-DHL-10 cells were seeded in 24-well plates at $1x10^5$ cells/well (n=5). The cells were then treated with increasing concentrations of curcumin (0, 10, 20, 40 and 60 μM). After 24 h, cell viability was measured using a CCK-8 assay according to the manufacturer's protocol. Specifically, 10 μl CCK-8 solution was added to each well and incubated for 1-1.5 h. Absorbance was measured at 450 nm using a microplate reader. Cell viability was calculated as: (ODsample-ODblank)/(ODcontrol-ODblank) x100%, with control groups set as 100% viability.

Cellular protein extraction. Following treatment, cells were collected by centrifugation at 200 x g for 5 min at 4˚C. The supernatant was discarded, and the cell pellet was washed with PBS, transferred to a new microcentrifuge tube and centrifuged again under the same conditions. The supernatant was then carefully removed. The cell pellet was resuspended in 70-110 μl ice-cold lysis buffer (Beyotime Biotechnology) supplemented with 1% protease and phosphatase inhibitors. The suspension was vortexed for 15 sec at 5 min intervals and incubated on ice for 30 min. The lysate was centrifuged at 15,000 x g for 20 min at 4˚C. The supernatant was collected, and the protein concentration was determined using a BCA protein assay kit (cat. no. 23227; Thermo Fisher Scientific, Inc.). Protein samples were mixed with 5X loading buffer (1:4 ratio) and denatured by heating at 95˚C for 10 min. Samples were either used immediately or stored at -80˚C for subsequent western blot analysis of relevant protein expression.

Cytoplasmic and nuclear protein isolation. Treated cells were collected by centrifugation at 200 x g for 5 min at 4˚C. After discarding the medium, the cell pellet was washed with PBS, transferred to a new tube and centrifuged as previously described. The supernatants were carefully aspirated. The pellet was resuspended in 200 μl ice-cold Cytoplasmic Extraction Reagent A (cat. no. P0028-1; Beyotime Biotechnology) containing 1% protease/phosphatase inhibitors, vortexed vigorously for 5 sec and incubated on ice for 15 min. Cytoplasmic Extraction Reagent B (10 μl) (cat. no. P0028-2; Beyotime Biotechnology) was added, followed by vortexing for 5 sec, incubation on ice for 1 min and vigorous shaking for 1 min. The tube was vortexed again for 5 sec and centrifuged at 14,000 x g for 10 min at 4˚C. The cytoplasmic supernatant was transferred to a pre-chilled tube for immediate use or storage at -80˚C. The nuclear pellet was washed three times with 200 μl ice-cold PBS by centrifugation at 3,000 x g (4˚C). The pellet was resuspended in 50 μl Nuclear Extraction Reagent (cat. no. P0028-3; Beyotime Biotechnology) with inhibitors and vortexed vigorously for 15-30 sec. The suspension was incubated on ice with intermittent vortexing (15-30 sec every 1-2 min) for 30 min. After centrifugation at 14,000 x g for 10 min (4˚C), the nuclear extract (supernatant) was collected. The protein concentrations of the cytoplasmic and nuclear fractions were determined separately using a BCA assay. The fractions were mixed with 5X loading buffer (1:4) and denatured at 95˚C for 10 min. Samples were used immediately or stored at -80˚C for analysis of nuclear translocation of proteins such as AIF and MIF.

Trypan blue exclusion assay. Cell suspensions were mixed with an equal volume of 0.4% trypan blue solution. A 10 μl aliquot was loaded onto a hemocytometer, incubated for 3 min at room temperature and viable cells were counted using an automated cell counter. Cell viability was expressed as a percentage of the control group (set as 100%). This was conducted for direct evaluation of the effects of curcumin and its combined treatments on cell viability.

Protein concentration determination by BCA assay. Protein concentrations were determined using the BCA assay to ensure consistent sample loading in western blot and related experiments, as detailed in the following protocol.

Briefly, a working solution was prepared by mixing the BCA reagents A and B in a 50:1 ratio. A standard curve was generated by adding 0-20 μg standard protein to a 96-well plate, followed by volume adjustment to 25 μl with deionized water. Subsequently, 2 μl each protein sample was loaded into the plate and also adjusted to 25 μl with deionized water. Then, 200 μl BCA working solution was added to each well, followed by incubation at 37˚C for 30 min protected from light. Finally, the absorbance was measured at 562 nm using a microplate reader, and sample protein concentrations were calculated based on a standard curve.

Western blot. Western blot was performed to detect the expression and localization changes of PAR polymers, PARP-1, AIF, MIF and apoptosis- and necroptosis-related proteins, following the detailed procedures below.

Whole-cell lysates were prepared using lysis buffer (Sigma-Aldrich; Merck KGaA) with 1% protease/phosphatase inhibitors on ice for 30 min, followed by centrifugation at 14,000 x g for 30 min at 4˚C. Protein concentration was determined using the BCA method. Nuclear and cytoplasmic fractions were isolated using a commercial extraction kit (cat. no. P0028; Beyotime Biotechnology) according to the manufacturer's instructions. Proteins (20 μg) were separated using 7.5, 10 and 12.5% SDS-PAGE gels according to their molecular sizes and transferred to PVDF membranes. Membranes were blocked with 5% skim milk and incubated with primary antibodies at 4˚C overnight. After washing with TBST (0.1% Tween, 3x10 min), the membranes were incubated with horseradish peroxidase-conjugated secondary antibodies (1:5,000; cat. nos. AS014 and AS0003; ABclonal Biotech. Co., Ltd.) for 1 h at room temperature. Signals were detected using an ECL substrate and a chemiluminescence imaging system (Tanon). The following primary antibodies were used: GAPDH

(1:10,000; cat. no. 600-GAPDHt; Trevigen Inc.), AIF (1:1,000; cat. no. #4642; Cell Signaling Technology, Inc.), MIF (1:1,000; cat. no. ab7207; Abcam), PAR (1:1,000; cat. no. #84510; Cell Signaling Technology, Inc.), PARP (1:1,000; cat. no. #9542; Cell Signaling Technology, Inc.), BCL-2 (1:1,000; cat. no. #3498; Cell Signaling Technology, Inc.), BCL-6 (1:1,000; cat. no. WL03134; Wanleibio Co., Ltd.), c-Myc (1:1,000; cat. no. A5011; Selleck Chemicals), Bax (1:1,000; cat. no. A19684; ABclonal Biotech Co., Ltd.), receptor interacting protein 1 (RIP1; 1:1,000; cat. no. #3493; Cell Signaling Technology, Inc.), receptor interacting protein 3 (RIP3; 1:1,000; cat. no. #13526; Cell Signaling Technology, Inc.), mixed lineage kinase domain like pseudokinase (MLKL; 1:1,000; cat. no. #14993; Cell Signaling Technology, Inc.), cleaved caspase-3 (1:1,000; cat. no. #9661; Cell Signaling Technology, Inc.) and caspase-3 (1:1,000; cat. no. #9662; Cell Signaling Technology, Inc.). Band intensities from three independent experiments were quantified using ImageJ 1.53t software (National Institute of Health).

Ultraviolet B (UVB) irradiation. UVB irradiation was employed to mimic the DNA-damaging stimuli of radiotherapy, thereby investigating the synergistic effects of curcumin combined with ultraviolet treatment. A Bio-Rad UVB irradiation system (Bio-Rad Laboratories, Inc.) was used, which emits ultraviolet light at wavelengths of 280-320 nm to generate UVB radiation. Before UVB exposure, the irradiation device was thoroughly sterilized with 75% ethanol. Subsequently, the cells were covered with 6-well plate lids and placed on a UV-transparent tray and irradiated at an intensity of 50 mJ/cm^2. Following UVB exposure, the cells were returned to the incubator for further incubation, allowing subsequent experiments to proceed. To ensure consistency and comparability in the present study and based on preliminary research findings (data not shown), the UVB irradiation time for SU-DHL-8 cells across all groups was set at 60 sec, whereas for SU-DHL-10 cells it was set at 120 sec across all groups.

Immunofluorescence staining. Immunofluorescence staining was conducted to directly visualize the subcellular localization of target proteins.

SU-DHL-10 cells (1x10^6 cells/ml) were seeded in 6-well plates and treated as indicated for 24 h. Cells were fixed with 4% paraformaldehyde (20 min, room temperature), permeabilized with 0.5% Triton X-100 (20 min) and washed with PBST. After blocking with 5% BSA (15 min, room temperature), cells were incubated with primary antibodies (AIF, cat. no. #4642; 1:50; PARP-1, cat. no. #9542; 1:200; Cell Signaling Technology, Inc.) overnight at 4˚C. The cells were then incubated with an FITC-conjugated secondary antibody (1:200; cat. no. AS014; ABclonal Biotechnology Co., Ltd.) for 1 h at room temperature counterstained with DAPI and mounted with an anti-fade reagent. Images were acquired using a fluorescence microscope (Nikon Corporation).

DAPI/PI staining. To distinguish between apoptotic and non-apoptotic cell death, cell death modalities were assessed via nuclear staining and membrane integrity markers. SU-DHL-10 cells (1x10^6 cells/ml) were seeded in 6-well plates, treated as indicated and incubated for 24 h. The cells were harvested and incubated in the dark at room temperature for 20 min with a solution containing DAPI (1:100 in PBS; Beijing Solarbio Science & Technology Co., Ltd.) and propidium iodide (PI; 1:20 in PBS; Beyotime Biotechnology). The cells were then washed three times with PBS. The stained cells were visualized using a fluorescence microscope (Nikon Corporation).

Statistics. Statistical analyses were performed using SPSS 22.0 (IBM Corp.) and GraphPad Prism 8.0.1 (Dotmatics). For comparisons among multiple groups, one-way analysis of variance (ANOVA) was used, followed by Tukey's HSD test for post hoc pairwise comparisons. Data are presented as the mean ± SD from at least three independent experiments. A P-value of <0.05 was considered statistically significant, and a P-value of <0.01 was considered highly statistically significant. All experiments were performed at least in triplicate.

Results

Curcumin induces non-apoptotic cell death. The effect of curcumin on DLBCL cell viability was assessed using the CCK-8 assay. Cells were treated with curcumin (0, 10, 20, 40 or 60 μmol/l) for 24 h. Curcumin significantly inhibited the viability of SU-DHL-8 and SU-DHL-10 cells in a concentration-dependent manner, with IC_{50} values of 22.12 and 39.22 μmol/l, respectively (Fig. 1A). To distinguish apoptotic from non-apoptotic cell death, the pan-caspase inhibitor Q-VD-OPh was used (44,45). Based on preliminary data and literature (45), cells were treated with 20 nmol/l Q-VD-OPh and 10 or 20 μmol/l curcumin for 24 h. In SU-DHL-8 cells, co-treatment with Q-VD-OPh (Cur20 + Q) significantly rescued cell viability compared with treatment with curcumin alone (Cur20). By contrast, Q-VD-OPh had no protective effect on SU-DHL-10 cells (Fig. 1B). Consistently, DAPI/PI staining showed a significant increase in stained cells after curcumin (20 μmol/l) treatment in both cell lines. This increase was attenuated by Q-VD-OPh in SU-DHL-8 cells, but not in SU-DHL-10 cells (Fig. 1C and D), indicating that curcumin-induced death in SU-DHL-10 cells was largely caspase-independent.

To investigate the mechanism of curcumin-induced cell death, the basal expression of c-Myc, BAX, BCL-2 and BCL-6 was examined. The effects of curcumin on caspase 3 and PARP-1 cleavage were assessed using western blotting. SU-DHL-10 cells lacked BAX expression, but showed higher levels of BCL-2, BCL-6 and c-Myc than SU-DHL-8 cells (Fig. 1E). Upon curcumin treatment, cleaved caspase-3 and cleaved PARP-1 levels significantly increased in SU-DHL-8 cells. This effect was suppressed by Q-VD-OPh. By contrast, cleaved caspase-3 and cleaved PARP-1 were undetectable in SU-DHL-10 cells under all conditions (Fig. 1G). These results confirmed that curcumin induces caspase-dependent apoptosis in SU-DHL-8 cells but triggers a non-apoptotic cell death pathway in SU-DHL-10 cells. Although RIP1 expression was higher in SU-DHL-10 cells, the key necroptosis mediators RIP3 and MLKL were expressed at very low levels (Fig. 1F), which is consistent with a previous report (46). Thus, necroptosis is unlikely to contribute to cell death in SU-DHL-10 cells.

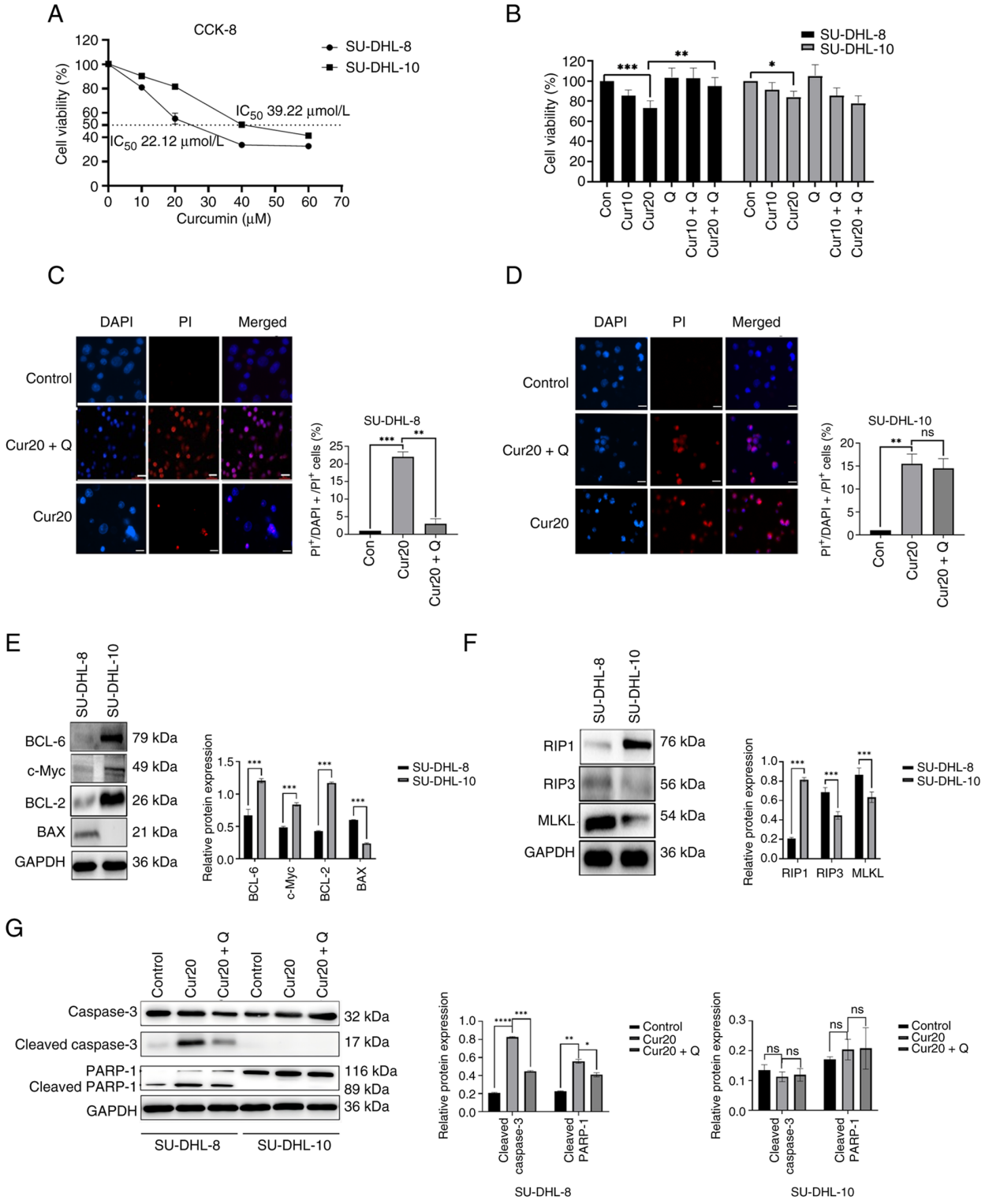

Figure 1. Curcumin induces non-apoptotic cell death. (A) Percentage cell viability after 0, 10, 20, 40 and 60 μM curcumin treatment for 24 h. (B) Cell viability percentage with or without curcumin or Q-VD-OPH for 24 h. Representative images of DAPI$^+$/PI$^+$ staining in (C) SU-DHL-8 and (D) SU-DHL-10 cells treated with curcumin ± Q-VD-OPH for 24 h. The percentage of DAPI$^+$/PI$^+$ staining cell in SU-DHL-8 and SU-DHL-10 cells treated with curcumin ± Q-VD-OPH for 24 h. (E) The protein levels of BAX, BCL-2, BCL-6 and c-Myc in SU-DHL-8 and SU-DHL-10 cells. (F) The protein levels of RIP1, RIP3 and MLKL in SU-DHL-8 and SU-DHL-10 cells. (G) The protein levels of cleaved caspase-3 and cleaved PARP-1 of SU-DHL-8 and SU-DHL-10 cells treated with 20 μM curcumin for 24 h. Scale bar, 25 μm. *P<0.05, **P<0.01,***P<0.001 and ****P<0.0001; ns, P≥0.05. Con, blank control group; Cur10, curcumin 10 μmol/l; Cur20, curcumin 20 μmol/l; Q, Q-VD-OPH; RIP, receptor interacting protein; PI, propidium iodide; MLKL, mixed lineage kinase domain like pseudokinase; PARP-1, poly(ADP-ribose) polymerase-1.

Curcumin causes the increase of PAR and upregulation of nuclear PARP1, AIF and MIF and nuclear translocation of AIF in DLBCL cells. To investigate the role of parthanatos, SU-DHL-10 cells were treated with 20 μM curcumin for 24 h, and the levels of PAR polymers were measured. The PARP-1 inhibitor olaparib (10 μM) and the pan-caspase

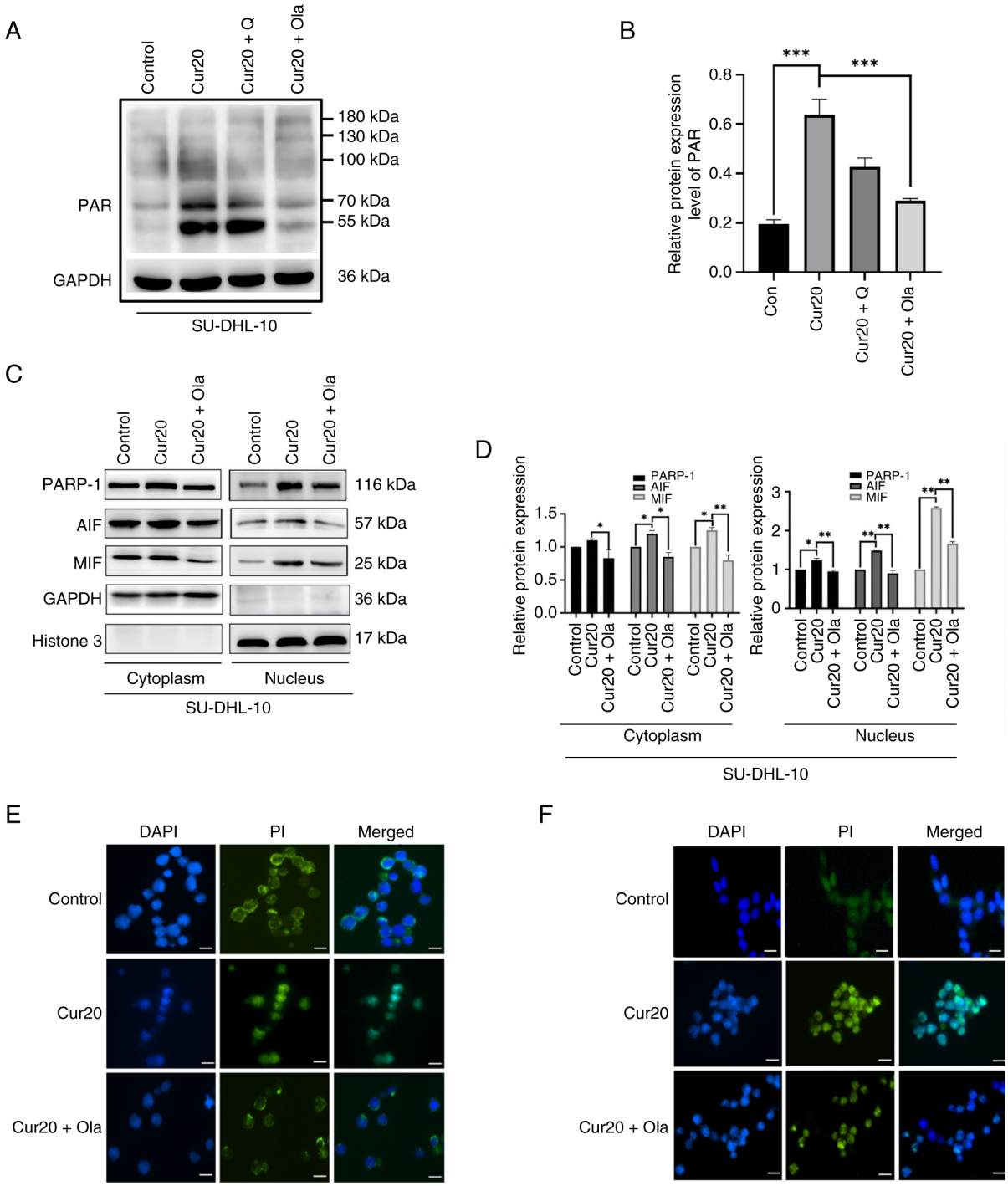

Figure 2. Curcumin causes the increase of PAR and upregulation of nuclear PARP-1, AIF and MIF, and nuclear translocation of AIF in DLBCL cells. (A) The protein level of PAR polymers in the SU-DHL-10 cells treated with 20 μM curcumin ± 20 nM Q-VD-OPh or 10 μM olaparib for 24 h (B) Relative protein expression levels of PAR in the SU-DHL-10 cells treated with 20 μM curcumin ± 20 nM Q-VD-OPh or 10 μM olaparib for 24 h. (C) The protein levels of PARP-1, AIFand MIF in the nucleus and cytoplasm of SU-DHL-10 cells treated with 20 μM curcumin ± 10 μM olaparib for 24 h. (D) Relative protein expression levels of PARP-1, AIF and MIF in the nucleus and cytoplasm of SU-DHL-10 cells treated with 20 μM curcumin ± 10 μM olaparib for 24 h. (E) Representative images of AIF immunofluorescence staining in SU-DHL-10 cells treated with 20 μM curcumin for 24 h. (F) Representative images of PARP-1 immunofluorescence staining in SU-DHL-10 cells treated with 20 μM curcumin for 24 h. *P<0.05, **P<0.01 and ***P<0.001; ns, P≥0.05. Scale bar, 25 μm. Cur20, curcumin 20 μmol/l; Q, Q-VD-OPH; Ola, olaparib; DLBCL, diffuse large B-cell lymphoma; PAR, poly(ADP-ribose); PARP-1, poly(ADP-ribose) polymerase-1; AIF, apoptosis-inducing factor; MIF, macrophage migration inhibitory factor; PI, propidium iodide.

inhibitor Q-VD-OPh (20 nM) were used for mechanistic validation. Western blot analysis showed a significant increase in PAR polymer levels in curcumin-treated SU-DHL-10 cells compared with those in the untreated control group (Fig. 2A and B). This increase was significantly suppressed by olaparib (Cur20 + Ola), but not by Q-VD-OPh (Cur20 + Q) (Fig. 2A and B). Furthermore, curcumin treatment significantly increased the nuclear protein levels of PARP-1, AIF and MIF, which were reversed by olaparib (Fig. 2C and D). Immunofluorescence staining consistently revealed the

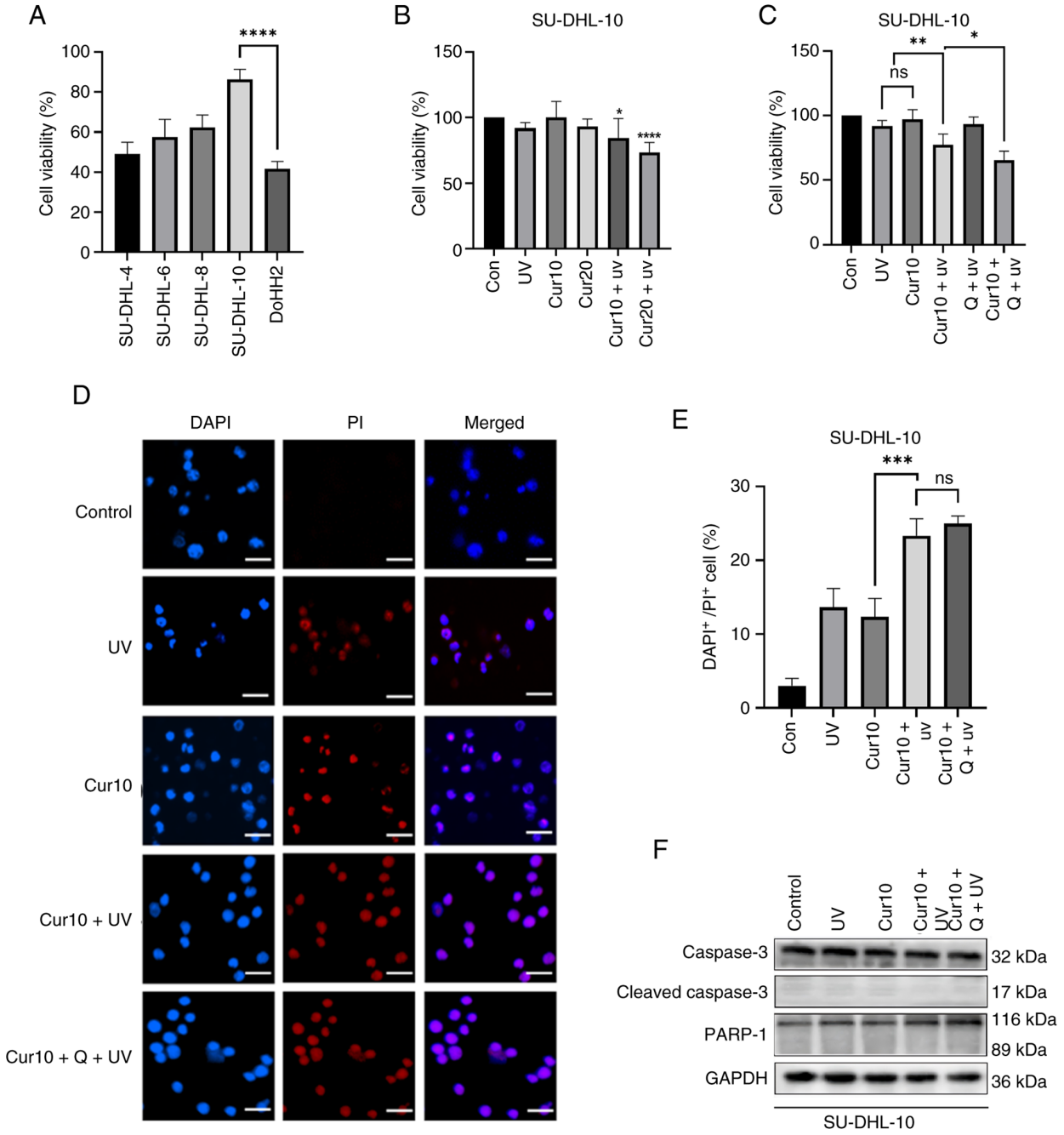

Figure 3. Curcumin combined with UVB induces non-apoptotic death. (A) Cell survival rates of different cell lines after UVB treatment. (B) Percentage of cell viability after 10 and 20 μM curcumin ± UVB treatment for 24 h. (C) Percentage of cell viability after 10 μM curcumin ± UVB or 20 nM Q-VD-OPh treatment for 24 h. (D) Representative images of $DAPI^+/PI^+$ staining in cells treated with curcumin ± UVB or 20 nM Q-VD-OPh for 24 h. (E) The percentage of $DAPI^+/PI^+$ staining cell in cells treated with 10 μM curcumin ± UVB or 20 nM Q-VD-OPh for 24 h. (F) The protein levels of cleaved caspase 3 and cleaved PARP-1 of cells treated with 10 μM curcumin ± UVB or 20 nM Q-VD-OPh for 24 h. *P<0.05, **P<0.01, ***P<0.001, ****P<0.0001 and ns, P≥0.05. Scale bar, 25 μm. Cur10, curcumin 10 μmol/l; Q, Q-VD-OPH; UVB, ultraviolet B radiation; PI, propidium iodide, PARP-1, poly(ADP-ribose) polymerase-1.

enhanced nuclear localization of both AIF and PARP-1 after curcumin treatment, which was attenuated by olaparib treatment (Fig. 2E and F).

Curcumin combined with UVB induces non-apoptotic death. SU-DHL-10 cells are relatively insensitive to DNA-damaging stimuli such as UVB (47) (Fig. 3A). To explore the combined effects of radiotherapy, SU-DHL-10 cells were treated with a low-dose of curcumin and UVB irradiation for 24 h. The CCK-8 assay showed that combined treatment with curcumin (10 or 20 μM) and UVB significantly reduced cell viability compared with single-agent treatments (Fig. 3B). Notably, the addition of Q-VD-OPh to the curcumin (10 μM) and UVB combination further decreased cell survival in the trypan blue exclusion assay (Fig. 3C). DAPI/PI staining confirmed a synergistic increase in cell death with the Cur10 + UV combination, which was not inhibited by Q-VD-OPh (Fig. 3D and E). Western blotting analysis confirmed the absence of cleaved caspase-3 and cleaved PARP-1 in cells treated with curcumin alone or in combination with UVB (Fig. 3F).

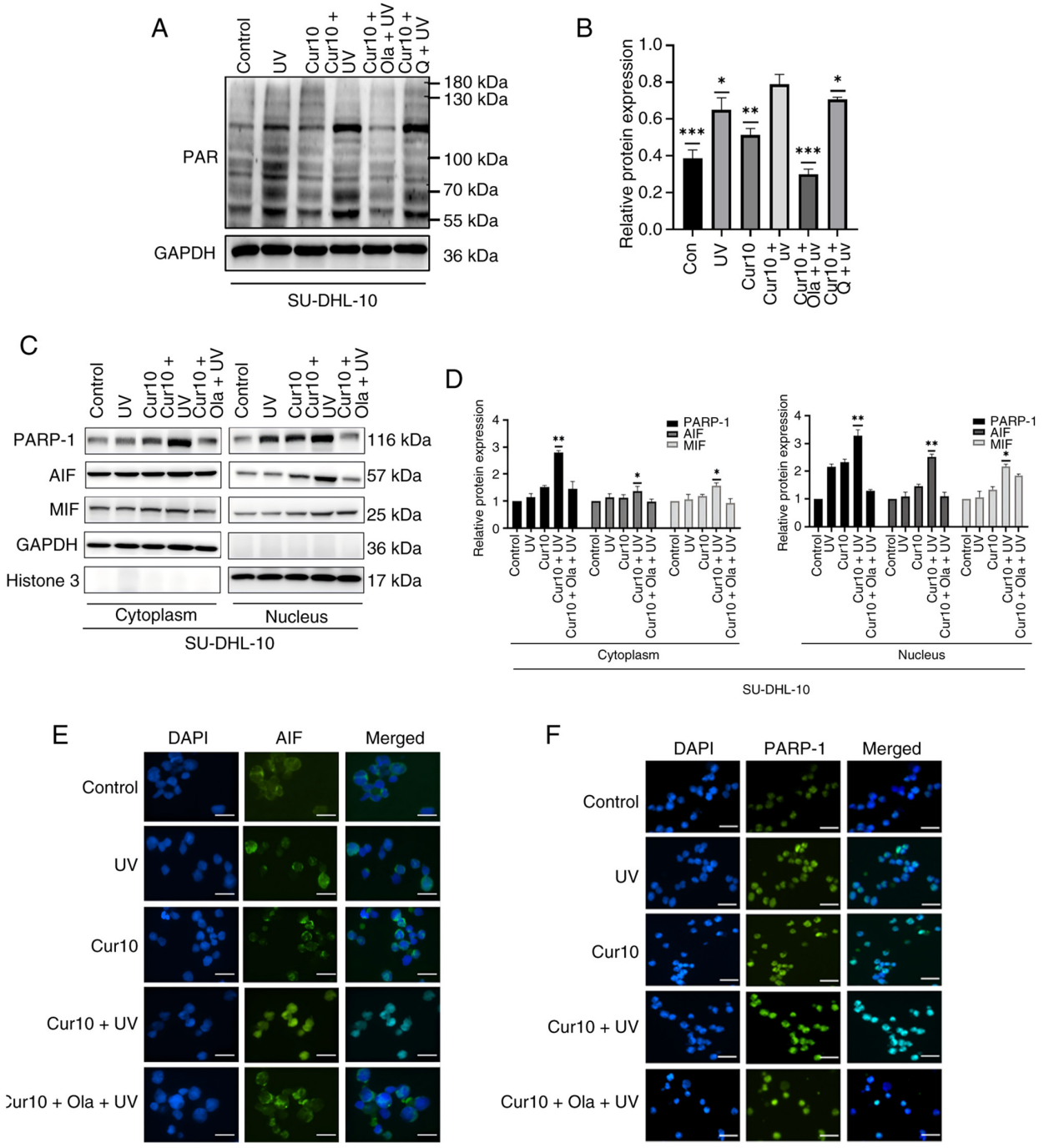

Figure 4. Curcumin sensitizes the antitumor effects of UVB through parthanatos. (A) The protein level of PAR polymers in the SU-DHL-10 cells treated with 10 μM curcumin combined UVB ± 20 nM Q-VD-OPh or 10 μM olaparib treatment for 24 h. (B) Relative protein expression levels of PAR in the SU-DHL-10 cells treated with 10 μM curcumin combined UVB ± 20 nM Q-VD-OPh or 10 μM olaparib treatment for 24 h. (C) The protein level of PARP-1, AIF and MIF in the nucleus and cytoplasm of SU-DHL-10 cells treated with 10 μM curcumin combined UVB ± 20 nM Q-VD-OPh or 10 μM olaparib treatment for 24 h. (D) Relative protein expression levels of PARP-1, AIF and MIF in the nucleus and cytoplasm of SU-DHL-10 cells treated with 10 μM curcumin combined UVB ± 20 nM Q-VD-OPh/10 μM olaparib treatment for 24 h. (E) Representative images of AIF immunofluorescence staining in SU-DHL-10 cells treated with 10 μM curcumin combined UVB ± 20 nM Q-VD-OPh/10 μM olaparib treatment for 24 h. (F) Representative images of PARP-1 immunofluorescence staining in SU-DHL-10 cells treated with 10 μM curcumin combined UVB ± 20 nM Q-VD-OPh/10 μM Olaparib treatment for 24 h. Scale bar, 25 μm. *P<0.05, **P<0.01 and ***P<0.001; ns, P≥0.05. Scale bar, 25 μm. Cur10, curcumin 10 μmol/l; Q, Q-VD-OPH; Ola, olaparib; UVB, ultraviolet radiation B; PAR, poly (ADP-ribose); PARP-1, poly (ADP-ribose) polymerase-1; AIF, apoptosis-inducing factor; MIF, macrophage migration inhibitory factor.

Curcumin sensitizes the antitumor effects of UVB through parthanatos. To determine whether parthanatos mediated the combined effect, PAR polymer expression was evaluated in SU-DHL-10 cells treated with curcumin and UVB. The PAR polymer levels were significantly higher in the Cur10 + UV group than in either treatment alone. Olaparib, but not Q-VD-OPh, effectively suppressed this increase (Fig. 4A and B). Furthermore, the nuclear levels of PARP-1, AIF and MIF were significantly elevated by the Cur10 + UV combination compared with the single treatments, and this elevation was reversed by olaparib (Fig. 4C and D). Immunofluorescence staining confirmed the enhanced nuclear

translocation of AIF and PARP-1 induced by the Cur10 + UV combination, which was inhibited by olaparib (Fig. 4E and F).

Discussion

In the present study, curcumin reduced the survival rate of SU-DHL-8 and SU-DHL-10 cells in a dose-dependent manner, and low-dose curcumin enhanced the cytotoxic effects of DNA-damaging agents (UVB irradiation) on the cells, consistent with the findings of Wang *et al* (48). In the CCK-8 assay, the cell survival rates in the SU-DHL-8 Cur10 and SU-DHL-10 Cur20 groups were significantly lower than those in the control group. Although a decrease was observed in the trypan blue exclusion assay, the difference was not statistically significant. The difference in the experimental principles between the two methods lies in the fact that cells that have lost viability or membrane integrity exhibit increased membrane permeability and are stained blue by trypan blue, whereas normal live cells with intact membrane structures exclude trypan blue, preventing it from entering the cell. In the CCK-8 assay, WST-8 was reduced by mitochondrial dehydrogenases in the presence of the electron carrier 1-methoxy-5-methylphenazinium methyl sulfate to form an orange-yellow soluble called formazan. The amount of formazan generated was proportional to the number and activity of viable cells. When the cell membrane is mildly damaged, but not to an extent that affects cell survival, the cells may not be stained or only lightly stained with trypan blue. Automated counting machines may consider these cells normal rather than damaged, resulting in the trypan blue exclusion assay being less sensitive than the CCK-8 assay (49,50). Furthermore, previous studies have shown that the CCK-8 assay is more sensitive than the trypan blue exclusion assay, which is consistent with the present experimental results.

Apoptosis resistance is a major clinical obstacle that contributes to the failure of traditional cancer therapies such as chemotherapy and radiotherapy, as well as the development of multidrug resistance. Developing novel anticancer agents or drug combination strategies that bypass the apoptotic pathway to induce cancer cell death is considered an effective approach to overcome this challenge (51,52). The present experimental results indicated that SU-DHL-10 cells did not express the crucial apoptosis-promoting protein BAX, yet exhibited high expression levels of c-Myc and the anti-apoptotic proteins BCL-2 and BCL-6. Curcumin was capable of inducing SU-DHL-10 cells death, and this process was not inhibited by the broad-spectrum caspase inhibitor Q-VD-OPh. The key molecular markers of apoptosis, cleaved caspase-3 and cleaved PARP-1, were not detected during this process. Furthermore, although SU-DHL-10 cells showed high of RIP1 expression, they also showed low RIP3 and MLKL expression. This finding is consistent with previous literature reporting that SU-DHL-10 does not express RIP3 or MLKL (38). RIP1, phosphorylated RIP3 and phosphorylated MLKL form the key complex of necroptosis (53). RIP3 and MLKL are indispensable molecules in this cell death pathway, and knockout or inhibition of both can impede the occurrence of necroptosis (54,55). Based on these observations, it was concluded that curcumin induced non-apoptotic cell death in SU-DHL-10 cells but did not induce necroptosis.

To the best of our knowledge, the present study is the first report demonstrating curcumin-induced activation of the parthanatos pathway in DLBCL cells. Curcumin significantly increased PAR polymer accumulation, an effect that was insensitive to Q-VD-OPh but was potently inhibited by the PARP-1 inhibitor olaparib. Furthermore, curcumin promoted the nuclear accumulation of PARP-1, AIF and MIF. Immunofluorescence analysis confirmed the enhanced nuclear translocation of PARP-1 and AIF, which was attenuated by olaparib treatment These findings align with the established hallmarks of parthanatos (56,57): Namely, cell death associated with excessive PAR polymer formation, which is dependent on PARP-1 activity (58).

Regarding the execution mechanism, AIF itself lacks nuclease activity, whereas MIF possesses both exonuclease and endonuclease activities capable of cleaving DNA. AIF binds to MIF in the cytoplasm to form a complex that, upon nuclear translocation, mediates large-scale DNA fragmentation and chromatin condensation upon its nuclear translocation leading to cell death (59). Notably, AIF is required for nuclear translocation of MIF, but not vice versa, highlighting the pivotal role of AIF in this process (60).

The clinical PARP inhibitor olaparib exerts its effects through mechanisms including inhibition of PARP enzymatic activity and 'trapping' of PARP-DNA complexes, leading to impaired DNA repair and genomic instability (61). In the context of parthanatos, olaparib blocks the downstream consequences of PARP-1 hyperactivation (61), thereby suppressing curcumin-induced PARP-1-dependent cell death induced by curcumin in SU-DHL-10 cells. Curcumin has been reported to synergize with radiotherapy and chemotherapy, often by promoting apoptotic cell death (62,63). Resistance to apoptosis is a major cause of treatment failure in conventional cancer therapies. Therefore, strategies that bypass apoptotic resistance by inducing alternative cell death pathways are of great therapeutic interest (64-66). In the present study, UVB radiation was used as a DNA-damaging stimulus, analogous to radiotherapy (67). Notably, curcumin can protect healthy tissues from UVB damage (68) while acting as a photosensitizer in tumor cells (69), suggesting a selective advantage. As anticipated, it was found that low-dose curcumin synergized with UVB to induce parthanatos in SU-DHL-10 cells. These results suggest that curcumin may serve as a radiosensitizer via the induction of parthanatos. However, translational studies are warranted to evaluate its clinical potential in combination with radiotherapy.

It is important to note that the present findings are primarily based on the SU-DHL-10 cell line, which serves as a model for high-risk, treatment-resistant DLBCL. This cell line models key features of resistance, including lack of BAX expression (68), low levels of key apoptotic (such as caspase-8) and necroptotic (such as RIP3 and MLKL) mediators (70,71), BCL-2 and MYC rearrangements characteristic of double-hit lymphoma (72,73) and inherent insensitivity to DNA damage (74). It should be noted that the SU-DHL-10 cell line used in the present study is a double-hit lymphoma model characterized by concurrent rearrangements in the MYC and BCL2 genes (75,76). Although the results obtained with this cell line are promising, their molecular profiles differ from those of major DLBCL subtypes such as germinal

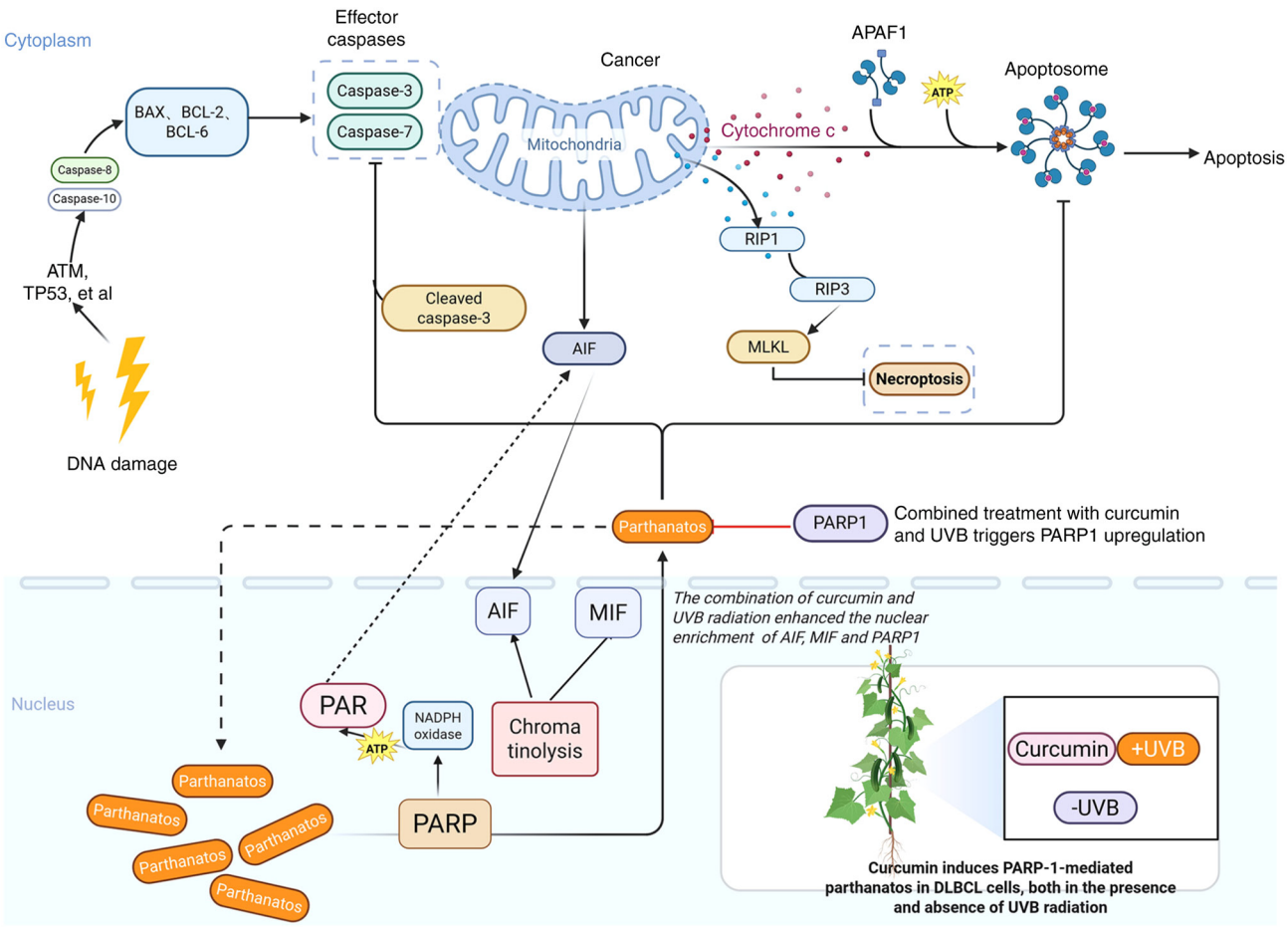

Figure 5. Schematic illustration of how curcumin ± UVB induces the PARP-1 mediated parthanatos in DLBCL. When cells undergo severe DNA damage, necroptosis can be mediated by RIP1, RIP3 and MLKL, and apoptosis can be induced by cleaved caspase-3 and cleaved PARP. However, SU-DHL-10 cells did not express RIP3 and MLKL, and no cleaved PARP was detected in the presence of curcumin ± UVB, so it was speculated that curcumin ± UVB did not cause necroptosis and apoptosis. On the contrary, curcumin ± UVB caused an increase in PAR polymer in SU-DHL-10 cells, and an increase in AIF and MIF in the nucleus, leading to chromatin shrinkage and DNA breakage, and eventually leading to parthanatos in DLBCL cells. DLBCL, diffuse large B-cell lymphoma; PAR, poly (ADP-ribose); PARP-1, poly (ADP-ribose) polymerase-1; AIF, apoptosis-inducing factor; MIF, macrophage migration inhibitory factor; UVB, ultraviolet radiation B; RIP, receptor interacting protein, MLKL, mixed lineage kinase domain like pseudokinase; BAX, Bcl-2-associated X protein; BCL, B-cell lymphoma 2; RIP, receptor-interacting protein kinase; ATP, adenosine triphosphate; APAF1, apoptotic protease activating factor 1; TP53, tumor protein p53.

center B-cell or activated B-cell lymphoma, which may limit the generalizability of the findings (77,78). Further validation using a broader panel of DLBCL cell lines representing distinct molecular subtypes, as well as primary patient-derived cells, is necessary to comprehensively assess the therapeutic potential of curcumin across heterogeneous DLBCL populations.

Curcumin, a multi-target natural compound, has demonstrated notable antitumor potential in preclinical studies DLBCL, particularly exhibiting a radiosensitizing effect when combined with radiotherapy (79-81). However, translating this potential into clinical practice faces multidimensional and complex challenges; for instance, curcumin exhibits extremely low oral bioavailability (typically <1%) due to its poor water solubility, low intestinal absorption rate and rapid hepatic first-pass metabolism (through reduction and conjugation) (82-85). Moreover, the complexity of the *in vivo* microenvironment may substantially influence these effects. DLBCL is highly heterogeneous, and different molecular subtypes may vary in their sensitivity to curcumin. Currently, most studies are based on single cell lines or animal models and lack stratified analyses across different patient subtypes. Consequently, it remains difficult to identify the optimal patient population that would benefit the most from curcumin combined with radiotherapy. Future research must advance synergistically across multiple fronts, including the optimization of drug delivery systems, in-depth elucidation of mechanisms of action, development of precise animal models and rigorous clinical trial designs, to gradually promote the clinical translation of curcumin in combination with radiotherapy for DLBCL (86-88). Future development of targeted delivery systems, such as the creation of curcumin nanocarriers that specifically accumulate in lymphoma lesions or lymph node regions (such as CD19/CD20-targeted nanoparticles), is key to achieving effective local radiosensitization while minimizing systemic toxicity (89-91). Concurrently, there is a need to leverage advanced preclinical models, such as patient-derived xenograft models or humanized mouse models, to more accurately simulate the radiation response and tumor microenvironment of DLBCL, thereby optimizing dosing regimens. Therefore, exploratory clinical trials should be conducted to systematically evaluate the safety, tolerability and preliminary efficacy of curcumin combined with

radiotherapy, while dynamically refining the timing and dosage ratios (86,92,93). In summary, translating the radiosensitizing effects of curcumin from the laboratory to clinical practice for DLBCL requires deep collaboration across multiple disciplines, including pharmaceuticals, radiation biology and hematologic oncology. It is hoped that curcumin-based combination regimens with novel targeted therapies or immunotherapies will demonstrate convincing synergistic effects in specific DLBCL subtypes, thereby offering patients with more effective and gentler treatment options.

In summary, the present study demonstrated that curcumin induced parthanatos in DLBCL cells through PARP-1 overactivation and AIF/MIF nuclear translocation. Furthermore, it exhibited synergistic cytotoxicity with UVB irradiation (Fig. 5). The present study provides a rationale for exploring parthanatos induction as a novel therapeutic strategy for R/R DLBCL and highlights the potential of curcumin as a radiosensitizer, which warrants further investigation.

Acknowledgements

The authors would like to thank Dr Zhen Yang (Tianjin Cancer Institute of Integrative Traditional Chinese and Western Medicine, Tianjin Union Medical Center of Nankai University, Tianjin, China) for their technical assistance and Dr Ruxue Liu (School of Integrative Medicine, Tianjin University of Traditional Chinese Medicine, Tianjin, China) for their helpful discussions and critical reading of the manuscript.

Funding

The present work was supported by the National Natural Science Foundation of China (grant no. 82070206) and Tianjin Key Medical Discipline Construction Project (grant no. TJYXZDXK-3-003A-5).

Availability of data and materials

The data generated in the present study may be requested from the corresponding author.

Authors' contributions

FL and HW contributed to the conceptualization of the study. YW, RQ and MQ were responsible for data curation, including organizing and verifying the research data. YW, RQ and XZ performed the formal analysis, applying statistical and analytical techniques to analyze the study data. MQ and HW acquired the funding that supported this research. YW, RQ and HM conducted the investigation, which involved performing the experiments and collecting the data. FL and HW developed the methodology, designing the procedures and frameworks used in the present study. MQ and HW handled project administration, coordinating and managing the research activities. FL and HW provided supervision, overseeing the research progress and providing guidance. YW was responsible for visualization, creating the figures and tables that present the data. YW and RQ wrote the original draft of the manuscript. YW, RQ and HW reviewed and edited the manuscript for important intellectual content. YW, MQ and HW confirm the authenticity of all the raw data. All authors read and approved the final version of the manuscript.

Ethics approval and consent to participate

Not applicable.

Patient consent for publication

Not applicable.

Competing interests

The authors declare that they have no competing interests.

Use of artificial intelligence tools

During the preparation of this work, artificial intelligence tools were used to improve the readability and language of the manuscript or to generate images, and subsequently, the authors revised and edited the content produced by the artificial intelligence tools as necessary, taking full responsibility for the ultimate content of the present manuscript.

References

1. Gong IY, Crump M, Prica A, Calzavara A, Liu N, Kordbacheh T, Rodin D, Hodgson D, Mozessohn L, Cheung MC and Kuruvilla J: Outcomes and factors influencing survival in patients with diffuse large B-cell lymphoma: A population-based analysis. Blood Neoplasia 2: 100117, 2025.
2. Nastoupil LJ and Bartlett NL: Navigating the evolving treatment landscape of diffuse large B-cell lymphoma. J Clin Oncol 41: 903-913, 2023.
3. He MY and Kridel R: Treatment resistance in diffuse large B-cell lymphoma. Leukemia 35: 2151-2165, 2021.
4. Liu Y, Stockwell BR, Jiang X and Gu W: p53-regulated non-apoptotic cell death pathways and their relevance in cancer and other diseases. Nat Rev Mol Cell Biol 26: 600-614, 2025.
5. Zhang Y, Zhang C, Li J, Jiang M, Guo S, Yang G, Zhang L, Wang F, Yi S, Wang J, *et al*: Inhibition of AKT induces p53/SIRT6/PARP1-dependent parthanatos to suppress tumor growth. Cell Commun Signal 20: 93, 2022.
6. Wang WQ, Liu L, Sun HC, Fu YL, Xu HX, Chai ZT, Zhang QB, Kong LQ, Zhu XD, Lu L, *et al*: Tanshinone IIA inhibits metastasis after palliative resection of hepatocellular carcinoma and prolongs survival in part via vascular normalization. J Hematol Oncol 5: 69, 2012.
7. Wang N, Chen S, Xie Y, Liu X, Xi Z, Li J, Xue C, Deng R, Min W, Kang R and Xie L: The Sanbi Decoction alleviates intervertebral disc degeneration in rats through intestinal flora and serum metabolic homeostasis modulation. Phytomedicine 127: 155480, 2024.
8. Ming T, Tao Q, Tang S, Zhao H, Yang H, Liu M, Ren S and Xu H: Curcumin: An epigenetic regulator and its application in cancer. Biomed Pharmacother 156: 113956, 2022.
9. Wang W, Li M, Wang L, Chen L and Goh BC: Curcumin in cancer therapy: Exploring molecular mechanisms and overcoming clinical challenges. Cancer Lett 570: 216332, 2023.
10. Abd El-Hack ME, El-Saadony MT, Swelum AA, Arif M, Abo Ghanima MM, Shukry M, Noreldin A, Taha AE and El-Tarabily KA: Curcumin, the active substance of turmeric: Its effects on health and ways to improve its bioavailability. J Sci Food Agric 101: 5747-5762, 2021.
11. Zhao PY, Ren H, Xu LY, Lou MF, Qing Y, Lin LT, Zhu ZP and Liao W: Research progress on pharmacological activity and mechanism of traditional Chinese medicine polysaccharides of *Curcuma*. Chin Tradit Herb Drugs 56: 5276-5287, 2025 (In Chinese).
12. Simamora A, Timotius KH, Yerer MB, Setiawan H and Mun'im A: Xanthorrhizol, a potential anticancer agent, from Curcuma xanthorrhiza Roxb. Phytomedicine 105: 154359, 2022.

13. Koh YC, Tsai YW, Lee PS, Nagabhushanam K, Ho CT and Pan MH: Amination potentially augments the ameliorative effect of curcumin on inhibition of the IL-6/Stat3/c-Myc pathway and gut microbial modulation in colitis-associated tumorigenesis. J Agric Food Chem 70: 14744-14754, 2022.
14. Chung SS, Dutta P, Chard N, Wu Y, Chen QH, Chen G and Vadgama J: A novel curcumin analog inhibits canonical and non-canonical functions of telomerase through STAT3 and NF-κB inactivation in colorectal cancer cells. Oncotarget 10: 4516-4531, 2019.
15. Siriviriyakul P, Chingchit T, Klaikeaw N, Chayanupatkul M and Werawatganon D: Effects of curcumin on oxidative stress, inflammation and apoptosis in L-arginine induced acute pancreatitis in mice. Heliyon 5: e02222, 2019.
16. Hu J, Lin S, Tan BK, Hamzah SS, Lin Y, Kong Z, Zhang Y, Zheng B and Zeng S: Photodynamic inactivation of Burkholderia cepacia by curcumin in combination with EDTA. Food Res Int 111: 265-271, 2018.
17. Aadinath W, Bhushani A and Anandharamakrishnan C: Synergistic radical scavenging potency of curcumin-in-β-cyclo dextrin-in-nanomagnetoliposomes. Mater Sci Eng C Mater Biol Appl 64: 293-302, 2016.
18. Zoi V, Galani V, Tsekeris P, Kyritsis AP and Alexiou GA: Radiosensitization and radioprotection by curcumin in glioblastoma and other cancers. Biomedicines 10: 312, 2022.
19. Ailioaie LM and Litscher G: Curcumin and photobiomodulation in chronic viral hepatitis and hepatocellular carcinoma. Int J Mol Sci 21: 7150, 2020.
20. Shetty NP, Prabhakaran M and Srivastava AK: Pleiotropic nature of curcumin in targeting multiple apoptotic-mediated factors and related strategies to treat gastric cancer: A review. Phytother Res 35: 5397-5416, 2021.
21. Deng L, Wu X, Zhu X, Yu Z, Liu Z, Wang J and Zheng Y: Combination effect of curcumin with docetaxel on the PI3K/AKT/mTOR pathway to induce autophagy and apoptosis in esophageal squamous cell carcinoma. Am J Transl Res 13: 57-72, 2021.
22. Calaf GM, Ponce-Cusi R and Carrión F: Curcumin and paclitaxel induce cell death in breast cancer cell lines. Oncol Rep 40: 2381-2388, 2018.
23. Lee YJ, Park KS and Lee SH: Curcumin targets both apoptosis and necroptosis in acidity-tolerant prostate carcinoma cells. Biomed Res Int 2021: 8859181, 2021.
24. Tang X, Ding H, Liang M, Chen X, Yan Y, Wan N, Chen Q, Zhang J and Cao J: Curcumin induces ferroptosis in non-small-cell lung cancer via activating autophagy. Thorac Cancer 12: 1219-1230, 2021.
25. Giordano A and Tommonaro G: Curcumin and cancer. Nutrients 11: 2376, 2019.
26. Rahman AT, Rafia R, Jethro A, Santoso P, Kharisma VD, Affan A, Murtadlo A, Purnamasari D, Soekamto NH, Ansori ANM, *et al*: In silico study of the potential of endemic sumatra wild turmeric rhizomes (curcuma sumatrana: Zingiberaceae) as anti-cancer. Pharmacogn J 14: 806-812, 2022.
27. Li K, Wang J, Xie Y, Lu Z, Sun W, Wang K, Liang J and Chen X: Reactive oxygen species/glutathione dual sensitive nanoparticles with encapsulation of miR155 and curcumin for synergized cancer immunotherapy. J Nanobiotechnology 22: 400, 2024.
28. Belcaro G, Hosoi M, Pellegrini L, Appendino G, Ippolito E, Ricci A, Ledda A, Dugall M, Cesarone MR, Maione C, *et al*: A controlled study of a lecithinized delivery system of curcumin (Meriva®) to alleviate the adverse effects of cancer treatment. Phytother Res 28: 444-450, 2014.
29. Pastorelli D, Fabricio ASC, Giovanis P, D'Ippolito S, Fiduccia P, Soldà C, Buda A, Sperti C, Bardini R, Da Dalt G, *et al*: Phytosome complex of curcumin as complementary therapy of advanced pancreatic cancer improves safety and efficacy of gemcitabine: Results of a prospective phase II trial. Pharmacol Res 132: 72-79, 2018.
30. Shah S, Rath H, Sharma G, Senapati SN and Mishra E: Effectiveness of curcumin mouthwash on radiation-induced oral mucositis among head and neck cancer patients: A triple-blind, pilot randomised controlled trial. Indian J Dent Res 31: 718-727, 2020.
31. Galluzzi L, Vitale I, Aaronson SA, Abrams JM, Adam D, Agostinis P, Alnemri ES, Altucci L, Amelio I, Andrews DW, *et al*: Molecular mechanisms of cell death: Recommendations of the nomenclature committee on cell death 2018. Cell Death Differ 25: 486-541, 2018.
32. Wang X, Zhang W, Ge P, Yu M and Meng H: Parthanatos participates in glutamate-mediated HT22 cell injury and hippocampal neuronal death in kainic acid-induced status epilepticus rats. CNS Neurosci Ther 28: 2032-2043, 2022.
33. Buckley AM, Lynam-Lennon N, O'Neill H and O'Sullivan J: Targeting hallmarks of cancer to enhance radiosensitivity in gastrointestinal cancers. Nat Rev Gastroenterol Hepatol 17: 298-313, 2020.
34. Tuo QZ, Zhang ST and Lei P: Mechanisms of neuronal cell death in ischemic stroke and their therapeutic implications. Med Res Rev 42: 259-305, 2022.
35. Liu S, Luo W and Wang Y: Emerging role of PARP-1 and PARthanatos in ischemic stroke. J Neurochem 160: 74-87, 2022.
36. So KY and Oh SH: Arsenite-induced cytotoxicity is regulated by poly-ADP ribose polymerase 1 activation and parthanatos in p53-deficient H1299 cells: The roles of autophagy and p53. Biochem Biophys Res Commun 656: 78-85, 2023.
37. Wen W, Jin K, Che Y, Du LY and Wang LN: Arnicolide D inhibits oxidative stress-induced breast cancer cell growth and invasion through apoptosis, ferroptosis, and parthanatos. Anticancer Agents Med Chem 24: 836-844, 2024.
38. Jiang X, Deng W, Tao S, Tang Z, Chen Y, Tian M, Wang T, Tao C, Li Y, Fang Y, *et al*: A RIPK3-independent role of MLKL in suppressing parthanatos promotes immune evasion in hepatocellular carcinoma. Cell Discov 9: 7, 2023.
39. Li C, Zhang J, Wu Q, Kumar A, Pan G and Kelvin DJ: Nifuroxazide activates the parthanatos to overcome TMPRSS2:ERG fusion-positive prostate cancer. Mol Cancer Ther 22: 306-316, 2023.
40. Liu L, Liu B, Guan G, Kang R, Dai Y and Tang D: Cyclophosphamide-induced GPX4 degradation triggers parthanatos by activating AIFM1. Biochem Biophys Res Commun 606: 68-74, 2022.
41. Boulos JC, Omer EA, Rigano D, Formisano C, Chatterjee M, Leich E, Klauck SM, Shan LT and Efferth T: Cynaropicrin disrupts tubulin and c-Myc-related signaling and induces parthanatos-type cell death in multiple myeloma. Acta Pharmacol Sin 44: 2265-2281, 2023.
42. Robinson N, Ganesan R, Hegedűs C, Kovács K, Kufer TA and Virág L: Programmed necrotic cell death of macrophages: Focus on pyroptosis, necroptosis, and parthanatos. Redox Biol 26: 101239, 2019.
43. Yang L, Guttman L, Dawson VL and Dawson TM: Parthanatos: Mechanisms, modulation, and therapeutic prospects in neurodegenerative disease and stroke. Biochem Pharmacol 228: 116174, 2024.
44. Kuželová K, Grebeňová D and Brodská B: Dose-dependent effects of the caspase inhibitor Q-VD-OPh on different apoptosis-related processes. J Cell Biochem 112: 3334-3342, 2011.
45. Caserta TM, Smith AN, Gultice AD, Reedy MA and Brown TL: Q-VD-OPh, a broad spectrum caspase inhibitor with potent antiapoptotic properties. Apoptosis 8: 345-352, 2003.
46. Bhatti IA, Abhari BA and Fulda S: Identification of a synergistic combination of Smac mimetic and Bortezomib to trigger cell death in B-cell non-Hodgkin lymphoma cells. Cancer Lett 405: 63-72, 2017.
47. Wang P, Wang P, Liu B, Zhao J, Pang Q, Agrawal SG, Jia L and Liu FT: Dynamin-related protein Drp1 is required for Bax translocation to mitochondria in response to irradiation-induced apoptosis. Oncotarget 6: 22598-22612, 2015.
48. Wang Z, Liu F, Liao W, Yu L, Hu Z, Li M and Xia H: Curcumin suppresses glioblastoma cell proliferation by p-AKT/mTOR pathway and increases the PTEN expression. Arch Biochem Biophys 689: 108412, 2020.
49. Miao Y, Zheng Y, Geng Y, Yang L, Cao N, Dai Y and Wei Z: The role of GLS1-mediated glutaminolysis/2-HG/H3K4me3 and GSH/ROS signals in Th17 responses counteracted by PPARγ agonists. Theranostics 11: 4531-4548, 2021.
50. Stepanenko AA and Dmitrenko VV: Pitfalls of the MTT assay: Direct and off-target effects of inhibitors can result in over/underestimation of cell viability. Gene 574: 193-203, 2015.
51. Moyer A, Tanaka K and Cheng EH: Apoptosis in cancer biology and therapy. Annu Rev Pathol 20: 303-328, 2025.
52. Tian X, Srinivasan PR, Tajiknia V, Sanchez Sevilla Uruchurtu AF, Seyhan AA, Carneiro BA, De La Cruz A, Pinho-Schwermann M, George A, Zhao S, *et al*: Targeting apoptotic pathways for cancer therapy. J Clin Invest 134: e179570, 2024.
53. Grootjans S, Vanden Berghe T and Vandenabeele P: Initiation and execution mechanisms of necroptosis: An overview. Cell Death Differ 24: 1184-1195, 2017.
54. Remijsen Q, Goossens V, Grootjans S, Van den Haute C, Vanlangenakker N, Dondelinger Y, Roelandt R, Bruggeman I, Goncalves A, Bertrand MJ, *et al*: Depletion of RIPK3 or MLKL blocks TNF-driven necroptosis and switches towards a delayed RIPK1 kinase-dependent apoptosis. Cell Death Dis 5: e1004, 2014.

55. Dondelinger Y, Aguileta MA, Goossens V, Dubuisson C, Grootjans S, Dejardin E, Vandenabeele P and Bertrand MJ: RIPK3 contributes to TNFR1-mediated RIPK1 kinase-dependent apoptosis in conditions of cIAP1/2 depletion or TAK1 kinase inhibition. Cell Death Differ 20: 1381-1392, 2013.
56. Li D, Kou Y, Gao Y, Liu S, Yang P, Hasegawa T, Su R, Guo J and Li M: Oxaliplatin induces the PARP1-mediated parthanatos in oral squamous cell carcinoma by increasing production of ROS. Aging (Albany NY) 13: 4242-4257, 2021.
57. Künzi L and Holt GE. Cigarette smoke activates the parthanatos pathway of cell death in human bronchial epithelial cells. Cell Death Discov 5: 127, 2019.
58. Wang HF, Wang ZQ, Ding Y, Piao MH, Feng CS, Chi GF, Luo YN and Ge PF: Endoplasmic reticulum stress regulates oxygen-glucose deprivation-induced parthanatos in human SH-SY5Y cells via improvement of intracellular ROS. CNS Neurosci Ther 24: 29-38, 2018.
59. Fatokun AA, Dawson VL and Dawson TM: Parthanatos: Mitochondrial-linked mechanisms and therapeutic opportunities. Br J Pharmacol 171: 2000-2016, 2014.
60. Wang Y, An R, Umanah GK, Park H, Nambiar K, Eacker SM, Kim B, Bao L, Harraz MM, Chang C, *et al*: A nuclease that mediates cell death induced by DNA damage and poly(ADP-ribose) polymerase-1. Science 354: aad6872, 2016.
61. Murai J, Huang SY, Das BB, Renaud A, Zhang Y, Doroshow JH, Ji J, Takeda S and Pommier Y: Trapping of PARP1 and PARP2 by clinical PARP inhibitors. Cancer Res 72: 5588-5599, 2012.
62. Lai X, Geng X, Li M, Tang M, Liu Q, Yang M, Shen L, Zhu Y and Wang S: Glutathione-responsive PLGA nanocomplex for dual delivery of doxorubicin and curcumin to overcome tumor multidrug resistance. Nanomedicine (Lond) 16: 1411-1427, 2021.
63. Zheng X, Yang X, Lin J, Song F and Shao Y: Low curcumin concentration enhances the anticancer effect of 5-fluorouracil against colorectal cancer. Phytomedicine 85: 153547, 2021.
64. Carneiro BA and El-Deiry WS: Targeting apoptosis in cancer therapy. Nat Rev Clin Oncol 17: 395-417, 2020.
65. Herrera M, Pretelli G, Desai J, Garralda E, Siu LL, Steiner TM and Au L: Bispecific antibodies: Advancing precision oncology. Trends Cancer 10: 893-919, 2024.
66. Sarmento-Ribeiro AB, Scorilas A, Gonçalves AC, Efferth T and Trougakos IP: The emergence of drug resistance to targeted cancer therapies: Clinical evidence. Drug Resist Updat 47: 100646, 2019.
67. Pollet M, Shaik S, Mescher M, Frauenstein K, Tigges J, Braun SA, Sondenheimer K, Kaveh M, Bruhs A, Meller S, *et al*: The AHR represses nucleotide excision repair and apoptosis and contributes to UV-induced skin carcinogenesis. Cell Death Differ 25: 1823-1836, 2018.
68. Ben Yehuda Greenwald M, Frušić-Zlotkin M, Soroka Y, Ben Sasson S, Bitton R, Bianco-Peled H and Kohen R: Curcumin protects skin against UVB-induced cytotoxicity via the keap1-Nrf2 pathway: The use of a microemulsion delivery system. Oxid Med Cell Longev 2017: 5205471, 2017.
69. Park K and Lee JH: Photosensitizer effect of curcumin on UVB-irradiated HaCaT cells through activation of caspase pathways. Oncol Rep 17: 537-540, 2007.
70. Galluzzi L, Kepp O, Chan FK and Kroemer G: Necroptosis: Mechanisms and relevance to disease. Annu Rev Pathol 12: 103-130, 2017.
71. Yuan J and Ofengeim D: A guide to cell death pathways. Nat Rev Mol Cell Biol 25: 379-395, 2024.
72. Zhang J, Wang T, Shetty K, Alkan S, Xu S, Gong Q, Liu X, Li Y, Hu Z, Huang W, *et al*: Genetic characterization and drug sensitivity study of newly derived HGBL double/triple-hit lymphoma cell lines. Blood Adv 6: 5067-5071, 2022.
73. Esteve-Arenys A, Valero JG, Chamorro-Jorganes A, Gonzalez D, Rodriguez V, Dlouhy I, Salaverria I, Campo E, Colomer D, Martinez A, *et al*: The BET bromodomain inhibitor CPI203 overcomes resistance to ABT-199 (venetoclax) by downregulation of BFL-1/A1 in in vitro and in vivo models of MYC+/BCL2+ double hit lymphoma. Oncogene 37: 1830-1844, 2018.
74. Ennishi D, Jiang A, Boyle M, Collinge B, Grande BM, Ben-Neriah S, Rushton C, Tang J, Thomas N, Slack GW, *et al*: Double-hit gene expression signature defines a distinct subgroup of germinal center B-cell-like diffuse large B-cell lymphoma. J Clin Oncol 37: 190-201, 2019.
75. Attieh M and Asakrah S: B-ALL with synchronous MYC and BCL-2 rearrangement. Blood 141: 1894, 2023.
76. Collinge B, Ben-Neriah S, Hilton LK, Alduaij W, Tucker T, Slack GW, Farinha P, Craig JW, Boyle M, Meissner B, *et al*: Unbalanced MYC break-apart FISH patterns indicate the presence of a MYC rearrangement in HGBCL-DH-BCL2. Blood 144: 1611-1616, 2024.
77. Chapuy B, Stewart C, Dunford AJ, Kim J, Kamburov A, Redd RA, Lawrence MS, Roemer MGM, Li AJ, Ziepert M, *et al*: Molecular subtypes of diffuse large B cell lymphoma are associated with distinct pathogenic mechanisms and outcomes. Nat Med 24: 679-690, 2018.
78. Schmitz R, Wright GW, Huang DW, Johnson CA, Phelan JD, Wang JQ, Roulland S, Kasbekar M, Young RM, Shaffer AL, *et al*: Genetics and pathogenesis of diffuse large B-cell lymphoma. N Engl J Med 378: 1396-1407, 2028.
79. Bozzuto G, Calcabrini A, Colone M, Condello M, Dupuis ML, Pellegrini E and Stringaro A: Phytocompounds and nanoformulations for anticancer therapy: A review. Molecules 29: 3784, 2024.
80. Qiao Q, Jiang Y and Li G: Curcumin improves the antitumor effect of X-ray irradiation by blocking the NF-κB pathway: An in-vitro study of lymphoma. Anticancer Drugs 23: 597-605, 2012.
81. Qiao Q, Jiang Y and Li G: Inhibition of the PI3K/AKT-NF-κB pathway with curcumin enhanced radiation-induced apoptosis in human Burkitt's lymphoma. J Pharmacol Sci 121: 247-256, 2013.
82. Pratama BP, Khairullah AR, Ma'ruf IF, Akintunde AO, Mustofa I, Mulyati S, Ahmad AZ and Ansori ANM: Revolutionizing curcumin bioavailability: From health benefits to placement in food packaging products. Food Syst 8: 343-354, 2025.
83. El-Saadony MT, Saad AM, Mohammed DM, Alkafaas SS, Ghosh S, Negm SH, Salem HM, Fahmy MA, Mosa WFA, Ibrahim EH, *et al*: Curcumin, an active component of turmeric: Biological activities, nutritional aspects, immunological, bioavailability, and human health benefits-a comprehensive review. Front Immunol 16: 1603018, 2025.
84. Heidari H, Bagherniya M, Majeed M, Sathyapalan T, Jamialahmadi T and Sahebkar A: Curcumin-piperine co-supplementation and human health: A comprehensive review of preclinical and clinical studies. Phytother Res 37: 1462-1487, 2023.
85. Matthewman C, Krishnakumar IM and Swick AG: Review: Bioavailability and efficacy of 'free' curcuminoids from curcumagalactomannoside (CGM) curcumin formulation. Nutr Res Rev 37: 14-31, 2024.
86. Zhang X, Cui Q, Yin L, Zhu J, Mao Y, Yin R, Shao H, Wang W, Sun X, Zhang Z, *et al*: Ginger-derived vesicle-like nanoparticles loaded with curcumin to alleviate ionizing radiation-induced intestinal damage via gut microbiota regulation. Gut Microbes 17: 2531210, 2025.
87. Sak K: Radiosensitizing potential of curcumin in different cancer models. Nutr Cancer 72: 1276-1289, 2020.
88. Sudarshan V, Shyamjith P, Kumar S, Ravindran F, Teraiya N, Choudhary B and Karki SS: Assessing the anti-leukemic efficacy of a curcuminoid in cellular and animal models. Eur J Med Chem 300: 118177, 2025.
89. Ipar VS, Dsouza A and Devarajan PV: Enhancing curcumin oral bioavailability through nanoformulations. Eur J Drug Metab Pharmacokinet 44: 459-480, 2019.
90. Zhao J, Jia W, Zhang R, Wang X and Zhang L: Improving curcumin bioavailability: Targeted delivery of curcumin and loading systems in intestinal inflammation. Food Res Int 196: 115079, 2024.
91. Chang R, Chen L, Qamar M, Wen Y, Li L, Zhang J, Li X, Assadpour E, Esatbeyoglu T, Kharazmi MS, *et al*: The bioavailability, metabolism and microbial modulation of curcumin-loaded nanodelivery systems. Adv Colloid Interface Sci 318: 102933, 2023.
92. Karimi A, Naeini F, Niazkar HR, Tutunchi H, Musazadeh V, Mahmoodpoor A, Asghariazar V, Mobasseri M and Tarighat-Esfanjani A: Nano-curcumin supplementation in critically ill patients with sepsis: A randomized clinical trial investigating the inflammatory biomarkers, oxidative stress indices, endothelial function, clinical outcomes and nutritional status. Food Funct 13: 6596-6612, 2022.
93. Karimi A, Pourreza S, Vajdi M, Mahmoodpoor A, Sanaie S, Karimi M and Tarighat-Esfanjani A: Evaluating the effects of curcumin nanomicelles on clinical outcome and cellular immune responses in critically ill sepsis patients: A randomized, double-blind, and placebo-controlled trial. Front Nutr 9: 1037861, 2022.